Click Here for Full Article

Magnetic character of a large continental transform: An aeromagnetic survey of the Dead Sea Fault

Uri S. ten Brink

U.S. Geological Survey, 384 Woods Hole Road, Woods Hole, Massachusetts 02543, USA (utenbrink@usgs.gov)

Michael Rybakov

Geophysical Institute of Israel, Lod 71100, Israel

Abdallah S. Al-Zoubi

Department of Surveying and Geomatics, Al–Balqa' Applied University, Salt 19117, Jordan

Yair Rotstein

Geophysical Institute of Israel, Lod 71100, Israel

Now at the U.S.–Israel Bi–national Science Foundation, Jerusalem 91450, Israel

[1] New high-resolution airborne magnetic (HRAM) data along a 120-km-long section of the Dead Sea Transform in southern Jordan and Israel shed light on the shallow structure of the fault zone and on the kinematics of the plate boundary. Despite infrequent seismic activity and only intermittent surface exposure, the fault is delineated clearly on a map of the first vertical derivative of the magnetic intensity, indicating that the source of the magnetic anomaly is shallow. The fault is manifested by a 10–20 nT negative anomaly in areas where the fault cuts through magnetic basement and by a <5 nT positive anomaly in other areas. Modeling suggests that the shallow fault is several hundred meters wide, in agreement with other geophysical and geological observations. A magnetic expression is observed only along the active trace of the fault and may reflect alteration of magnetic minerals due to fault zone processes or groundwater flow. The general lack of surface expression of the fault may reflect the absence of surface rupture during earthquakes. The magnetic data also indicate that unlike the San Andreas Fault, the location of this part of the plate boundary was stable throughout its history. Magnetic anomalies also support a total left-lateral offset of 105–110 km along the plate boundary, as suggested by others. Finally, despite previous suggestions of transtensional motion along the Dead Sea Transform, we did not identify any igneous intrusions related to the activity of this fault segment.

1. Introduction

[2] Fault zones at depth are sometimes viewed as having a narrow (~1−2 m) core zone, where much of the slip is accommodated [*Chester et al.*, 1993]. However, the uppermost sediments and crystalline basement often have higher density of fractures and pores than the underlying crust, and friction may increase with sliding velocity on the fault (velocity strengthening), thus preventing rupture during an earthquake [*Marone*, 1998]. *Savage and Lisowski* [1993] suggested that the uppermost part of the fault plane often creeps and partially accommodates the secular slip rate on the fault. InSAR data associated with the 2003 Bam, Iran, earthquake indicate a lack of coseismic deformation in the vicinity of the fault, suggesting that inelastic deformation may take place in the top 2 km of the crust during the inter-seismic period [*Fialko et al.*, 2005].

[3] Continental transform faults, such as the Anatolian, the Dead Sea, and the San Andreas faults, provide a simple setting for studies of shallow fault zone rheology and deformation, due to their long-term activity at relatively narrow zones. Geophysical work across the San Andreas Fault in central California shows a 1-km wide zone of relatively low velocity, high electrical conductivity, and low density immediately southwest of the active fault trace, which extends from the surface to a depth of 1−3 km [*Hole et al.*, 2001, and references therein]. Characterization of the shallow structure of the Arava (Araba) Fault, a segment of the Dead Sea Transform, has yielded conflicting results about the width of that fault. Analysis of trapped seismic waves at Lat. 30°34′N (about 24 km north of the northern end of the survey area, Figure 1b) shows a 3−12 m wide low-velocity zone reaching a depth of 300 m under the surface trace of the fault [*Haberland et al.*, 2003]. High-resolution seismic reflection profiles across the fault, reveal, however, several parallel fault traces, interpreted as either a network of anastamosing faults at different scales or a surficial expression of secondary faults that merge to a single fault at depth [*Haberland et al.*, 2007]. A similar observation was recorded at the southern end of our survey area (~29°40′N [*Shtivelman et al.*, 1998]). Geological studies at Lat. 30°34′N and 30°49.4′N indicate a ~300 m wide fault zone, which lacks a defined core zone [*Janssen et al.*, 2004]. The damaged zone consists of small faults, fractures, striations, veins, and calcite twins. Steeply dipping scarps and vegetation lines are observed in places on the surface and on satellite photos [*Kesten*, 2004]. Geochemical analysis indicates that fluids entered the damaged zone from the surrounding sediments at shallow levels, perhaps to replace co-seismic fluid expulsion [*Janssen et al.*, 2004]. Magnetotelluric measurements in the same area (Lat. 30°34′N) do not reveal a high-conductivity zone associated with the fault [*Ritter et al.*, 2003] in contrast to the San Andreas Fault in central California [*Unsworth et al.*, 2000]. Instead, the fault zone appears to be a boundary between zones of low and high conductivities [*Ritter et al.*, 2003]. An absence of coherent near-surface seismic reflectivity was noted in seismic reflection data within an 800-m-wide zone at 30°30′N [*Kesten*, 2004].

[4] The 1000-km-long Dead Sea fault system accommodates left-lateral slip between the Arabian and African plates (Figure 1). The total slip along the fault system is 105−110 km over the past 16−18 m.y. [*Quennell*, 1958; *Freund et al.*, 1970]. The present slip rate is 4 mm/y [*Wdowinski et al.*, 2004; *Mahmoud et al.*, 2005], and the last damaging earthquake in the area was in AD 1458 [*Klinger et al.*, 2000a]. We report here the results of a high-resolution airborne magnetic survey along a 120-km-long segment of the Arava (Araba) Fault immediately north of the Gulf of Aqaba (Elat). The fault has no clear surface expression in the majority of this area, and hence its actual location is still debated [e.g., *ten Brink et al.*, 1999; *Frieslander*, 2000]. Micro-seismic activity is too sparse to provide information about the fault location and geometry [e.g., *Aldersons et al.*, 2003]. Here, we demonstrate the utility of high-resolution magnetic surveys, which are relatively simple and inexpensive to conduct, to the mapping of continental transform faults, and discuss the implications of the results to the understanding of the shallow structure of the Dead Sea transform.

[5] The fault and the valley along which the Dead Sea Transform passes, are called Arava in Israel and Araba in Jordan, and the Gulf is referred to as Elat in Israel and Aqaba in Jordan. In this paper we will use the terms that are used more commonly in the literature, Arava fault and valley, and the Gulf of Aqaba.

2. Data

[6] We conducted a high-resolution aeromagnetic (HRAM) survey in 2003 aboard a Royal Jordanian Air Force helicopter with technical assistance from Sander Geophysics Limited. The survey block is situated in the south of Jordan and Israel, within the Arava Valley and extends from the Gulf of
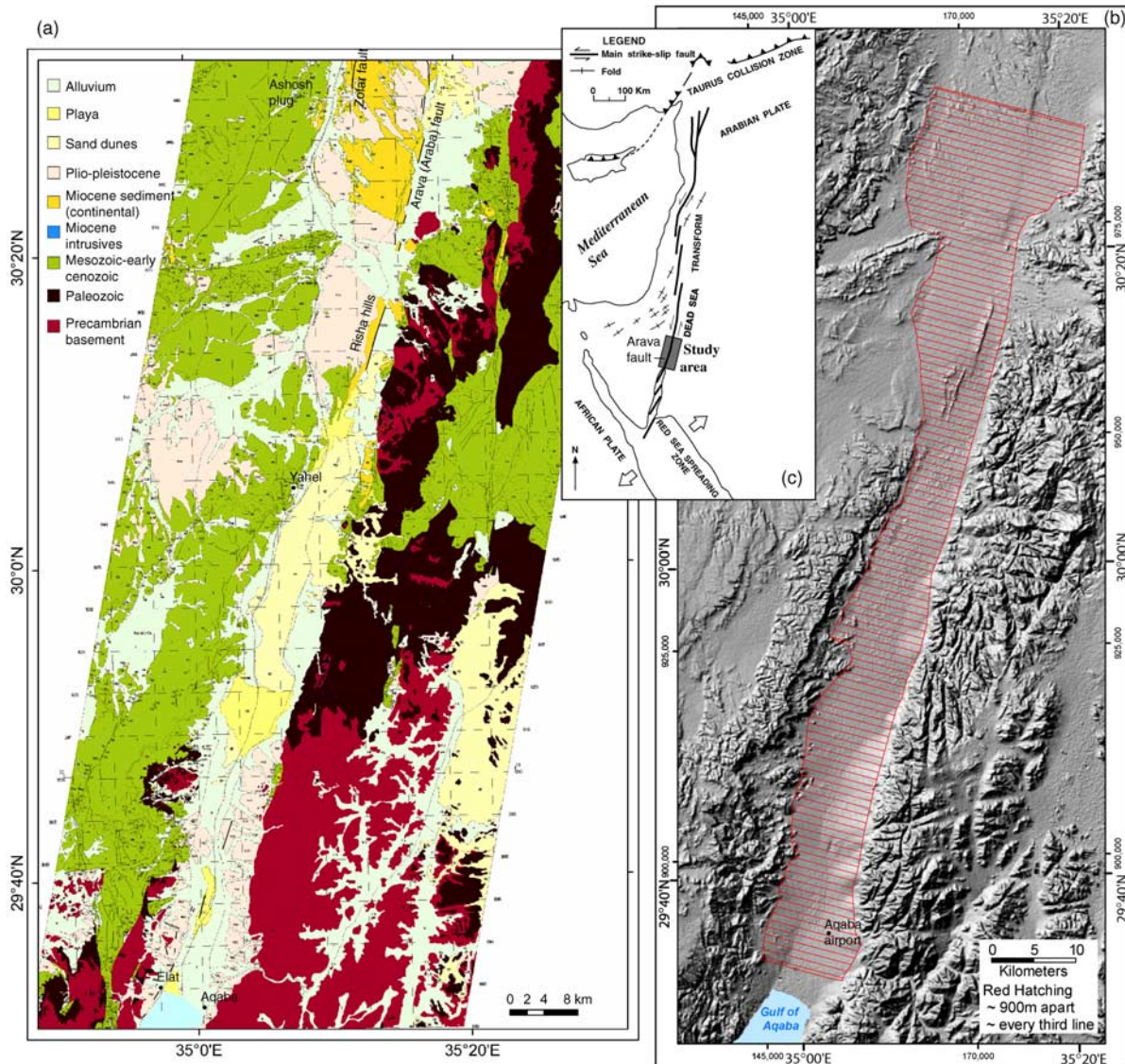
Figure 1. (a) Geological map of the southern Arava (Araba) valley simplified from [*Sneh et al.*, 1998]. Black lines, surface expression of faults [from *Sneh et al.*, 1998]. (b) Survey area and flight lines (every third shown) superposed on shaded relief of the topography. (c) General tectonic map of the Dead Sea transform.

Aqaba about 120 km to the north (Figure 1). The topography is generally flat within the valley, with steep mountains rising on either side. The survey block is arid with only sparse vegetation. The survey design required frequent crossings of the international border between Israel and Jordan.

[7] Survey operations were conducted from the Aqaba International Airport, Jordan, near the southern end of the survey area. The survey was flown along parallel lines spaced 300 m apart and oriented 105°E. Control lines were spaced 1,000 m apart and oriented at 15°E (Figure 1). The helicopter flew at an altitude of 128 ± 20 m above terrain. The magnetometer was mounted in a fiberglass "bird"

and towed roughly 25 m below the helicopter; hence the mean terrain clearance was ~100 m. Flying speed was on average 40 m/s (144 km/h). Magnetic measurements were recorded every 0.5 s, nominally at 20 m intervals. A total of 209,350 magnetic measurements were collected along 4,187 km of survey lines. A ground station magnetometer sensor was mounted on a 2-m high pole by the airport and recorded the magnetic field every 0.5 s. The noise level of the base station was less than 0.1 nT. Both the ground and airborne systems used a non-oriented (strap-down) optically pumped cesium split-beam magnetic sensor, with a sensitivity of 0.005 nT, a range of 15,000 to 100,000 nT, and a

sensor noise of less than 0.02 nT. A GPS receiver automatically provided the time base and location at 1 s interval for both the ground and airborne systems, ensuring accurate synchronization of the two data sets. Post-processed differential GPS corrections were applied to all survey lines using a ground-based GPS station at the Aqaba International Airport. The position of the ground station was determined by applying differential corrections with respect to IGS reference stations in Israel and Turkey. The estimated receiver location accuracy is ±0.2 m. Location was referenced to the WGS-84 ellipsoid.

[8] Time-varying magnetic measurements at the ground station magnetometer were corrected for the International Geomagnetic Reference Field (IGRF) 2000 model using the fixed ground station location and the recorded date for each flight. The airborne magnetometer data were also adjusted for IGRF, using the location, altitude, and date of each datum. Airborne magnetometer data were filtered for spikes and noise. Data were corrected for diurnal variations by subtracting the IGRF corrected ground station data and adding the average residual ground station value (-52.28 nT). The average ground station value was calculated from all the ground station data used to correct the airborne data, ensuring that the ground station corrections did not bias the airborne data set. As part of the leveling procedure, differences in intersections between control and traverse lines were minimized. The leveling procedure was checked by inspection of grids of the total magnetic intensity (TMI) and the first vertical derivative of the total magnetic intensity (FVD). Leveling statistics were also examined to ensure that steep correction gradients were minimized. The magnetic data were then gridded at 75 m intervals, reduced to pole, and incorporated into a GIS together with elevation, geology, and gravity maps to facilitate interpretation.

3. Interpretation

[9] The major findings from the new high-resolution aeromagnetic data are as follows: (1) An almost continuous transform fault follows the axis of the transform valley, and is expressed by a magnetic anomaly several hundred meters wide. (2) Long wavelength magnetic anomalies within the transform valley are continuous with anomalies west of the valley, but not with anomalies east of the valley, indicating that motion in this segment of the transform has always been confined to the active trace of the fault or distributed farther east. (3) There does not appear to be transform-fault related igneous activity in this segment of the transform valley. The following is a detailed discussion of the results.

3.1. Detection of the Arava Fault With Magnetic Data

[10] The Arava fault trace can be observed on the high-resolution magnetic data, particularly on a map of the first-vertical derivative (FVD) of the total magnetic intensity field (TMI) (Figure 2). The FVD emphasizes anomalies of shallow origin, because the field is inversely proportional to the square of the distance from the observation point to the source; hence moving toward a shallow source will produce a larger change in the anomaly than moving toward a deep source [e.g., *Blakely*, 1995]. The TMI field was reduced to pole prior to extracting the derivative, in an attempt to place the anomalies in their proper locations. Reduction to the pole removes asymmetries from magnetic anomalies, caused by non-vertical magnetizations and the regional field [e.g., *Blakely*, 1995, pp. 330–332].

[11] The fault appears in the magnetic data as an almost continuous trace within the transform valley, with the exception perhaps of a small (1–3 km) jog at the center of the survey area. The magnetic trace generally coincides with the location of the fault trace from surficial lineaments and pressure ridges, truncations or offsets of alluvial fans, [*Garfunkel et al.*, 1981; *Sneh et al.*, 1998; *Ginat et al.*, 1998; *Klinger et al.*, 2000b] (Figures 1 and 2), and from seismic reflection data [*Shtivelman et al.*, 1998; *Frieslander*, 2000]. The magnetic expression of the fault is remarkable because most of the transform valley appears to be devoid of magmatic bodies and is covered by relatively non-magnetic alluvial

Figure 2. (a) Total magnetic intensity (TMI) field, which was reduced to pole, superposed on shaded relief of the topography. Contour interval, 20 nT. Solid lines, location of profiles in Figures 4–6. (b) Contours of the Bouguer gravity anomaly map [after *ten Brink et al.*, 1999], superposed on the total magnetic intensity (TMI) field, which was reduced to pole. Contour interval of the Bouguer gravity anomaly is 2 mGal. (c) First vertical derivative (FVD) of the total magnetic intensity (TMI) field (reduced to pole). Solid lines, interpreted fault traces from the magnetic data. (d) Shaded relief of the FVD map illuminated from the west to highlight the fault trace. The linear high-amplitude anomalies in the southwest part of the survey area in Figures 2c and 2d are due to high-voltage power lines.
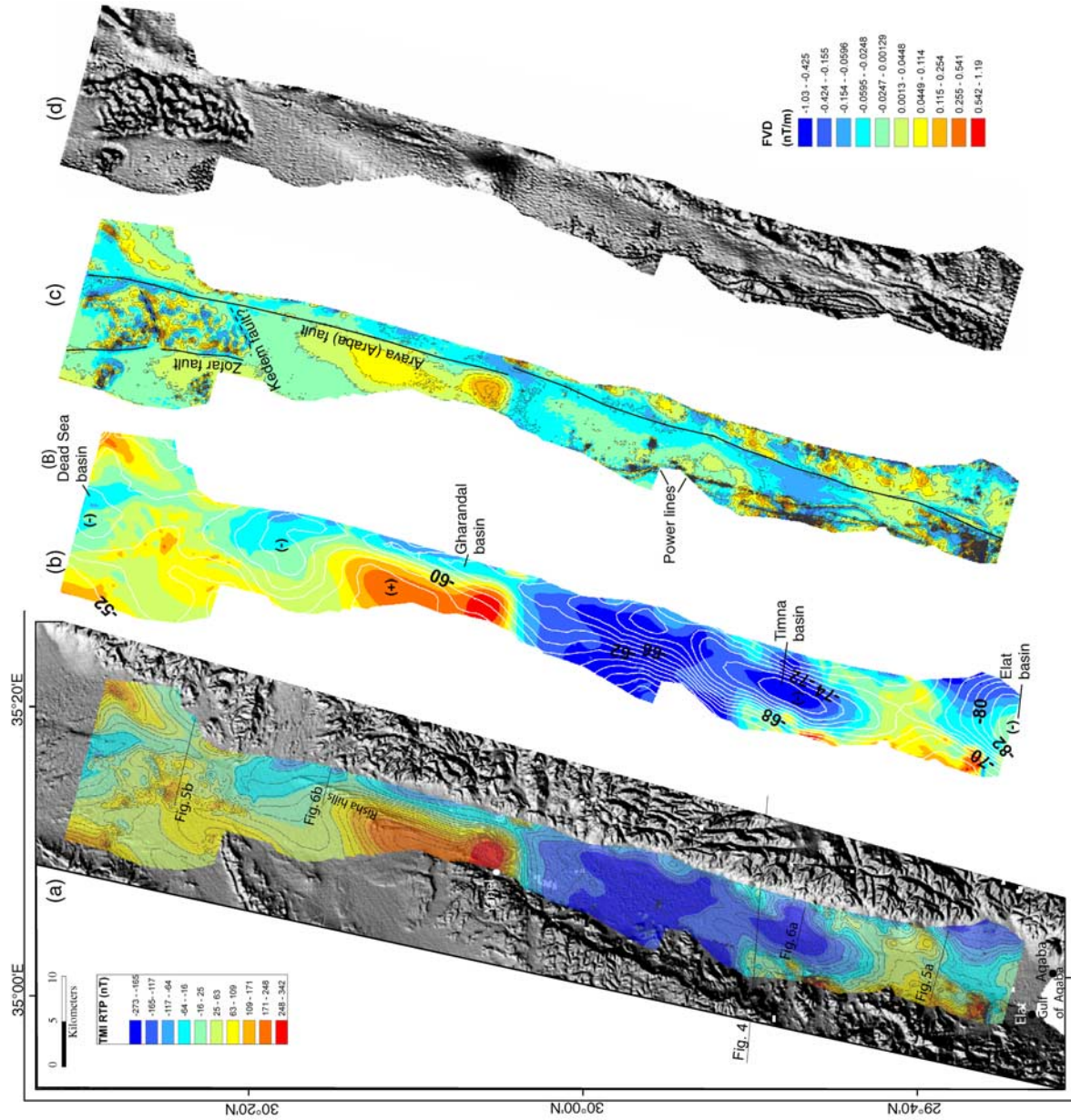
Figure 2

sediments and mud flats of varying thickness [e.g., *Sneh et al.*, 1998].

3.2. Regional Magnetic Anomalies and the Arava Fault

[12] The long wavelength anomalies of the magnetic intensity field often correspond to deeper crustal sources. These anomalies are emphasized in the TMI data which were continued upward to an elevation of 3000′ (900 m) above sea level and placed between a regional magnetic survey that was previously flown at that elevation in Israel [*Domzalski*, 1967] and a regional magnetic survey that was previously flown at elevations of 1500–2000 m above sea level in Jordan [*Hatcher et al.*, 1981; *Al-Zoubi and Ben-Avraham*, 2002] (Figure 3). (The eastern highlands are significantly higher in elevation than both the transform valley and the western highlands; hence terrain clearance there is only several hundred meters).

[13] The most striking observation about these anomalies is their continuation from the west into the transform valley, and their abrupt termination along the eastern side of the valley in the vicinity of the Arava Fault trace (Figure 3a). This observation indicates that with the exception of the southernmost survey area, at no time in the history of the Dead Sea Transform has significant relative plate motion in this part of the transform been accommodated along the western part of the transform valley or within the western highlands. This is in contrast to other intracontinental transform faults, such as the San Andreas Fault, where the plate boundary is 100s of km wide, and may indicate a rigid, relatively homogenous crust in this segment of the Dead Sea Transform. This finding is inconsistent with previous interpretations based on seismic reflection profiles across the western side of the valley that place a major fault there [e.g., *Frieslander*, 2000]. The seismic reflection profiles illuminate steeply dipping faults, which we interpret as secondary faults along the western edges of subsurface basins. On the other hand, it is possible

that some past relative motion was accommodated in the eastern highlands within 30 km of the present trace of Arava fault [*Kesten*, 2004]. The linear eastern edge of the transform valley, which includes small trapped grabens (Figure 1), was interpreted as a normal fault with an unknown amount of strike slip motion [*Garfunkel et al.*, 1981; *Frieslander*, 2000]. In fact, the regional anomaly in the southern half of the survey area is discontinuous across the eastern edge of the transform valley even after restoration of the eastern highlands to their pretransform position 111 km southward (Figure 3b).

[14] An east-west negative anomaly, located between lat. 29°47′–30°3′N, is bordered in the north and the south by positive anomalies. It probably reflects contrasts in magnetic properties of the buried crystalline basement dating to the Precambrian [*Segev et al.*, 1999]. These negative and positive anomalies extend eastward across the transform valley 111 km to the north, providing clear evidence for the total motion along the Dead Sea Transform [*Hatcher et al.*, 1981; *Rybakov et al.*, 1997] (Figure 3b).

[15] As discussed in the next section, some geological markers and magnetic anomalies match better with an offset of 107 km, while others with an offset 111 km; thus a single offset value could not be found. Analyses of other geological markers have put the total displacement of the Dead Sea Transform at between 105 and 110 km from. [*Quennell*, 1958; *Freund et al.*, 1970; *Garfunkel*, 1981]. The discrepancy between the values is due to the recent sediments covering the transform valley and obscuring the underlying geology, and the possibility of several parallel fault strands in some areas along which displacement has occurred in the past.

3.3. Origin of Magnetic Anomalies Within the Arava Valley

[16] The rift-like morphology of the Dead Sea Transform has led to suggestions of magmatic upwelling

Figure 3. Total magnetic intensity map of the survey area upward continued to an elevation of 900 m and plotted with existing regional magnetic maps from Israel [*Domzalski*, 1967] and Jordan [*Hatcher et al.*, 1981; *Al-Zoubi and Ben-Avraham*, 2002]. Contour interval, 20 nT. Solid line, trace of the Arava (Araba) Fault based on Figure 2d. The discrepancy between the upward continued survey data in the transform valley and the regional maps of Jordan and Israel is due to the different acquisition times and parameters of each data set. (b) Same as Figure 3a with the eastern side of the map shifted southward by 111 km along the Arava Fault to produce a continuous north-south gradient in the regional magnetic field at 30°0′N. Solid line, trace of the Arava Fault based on Figure 2d. (c) First vertical derivative of the total magnetic intensity field (reduced to pole) superposed on a simplified geological map of the area [*Sneh et al.*, 1998]. The area east of Arava Fault is restored to its pretransform position by shifting it southward by 107 km, following *Quennell* [1958] and *Freund et al.* [1970].
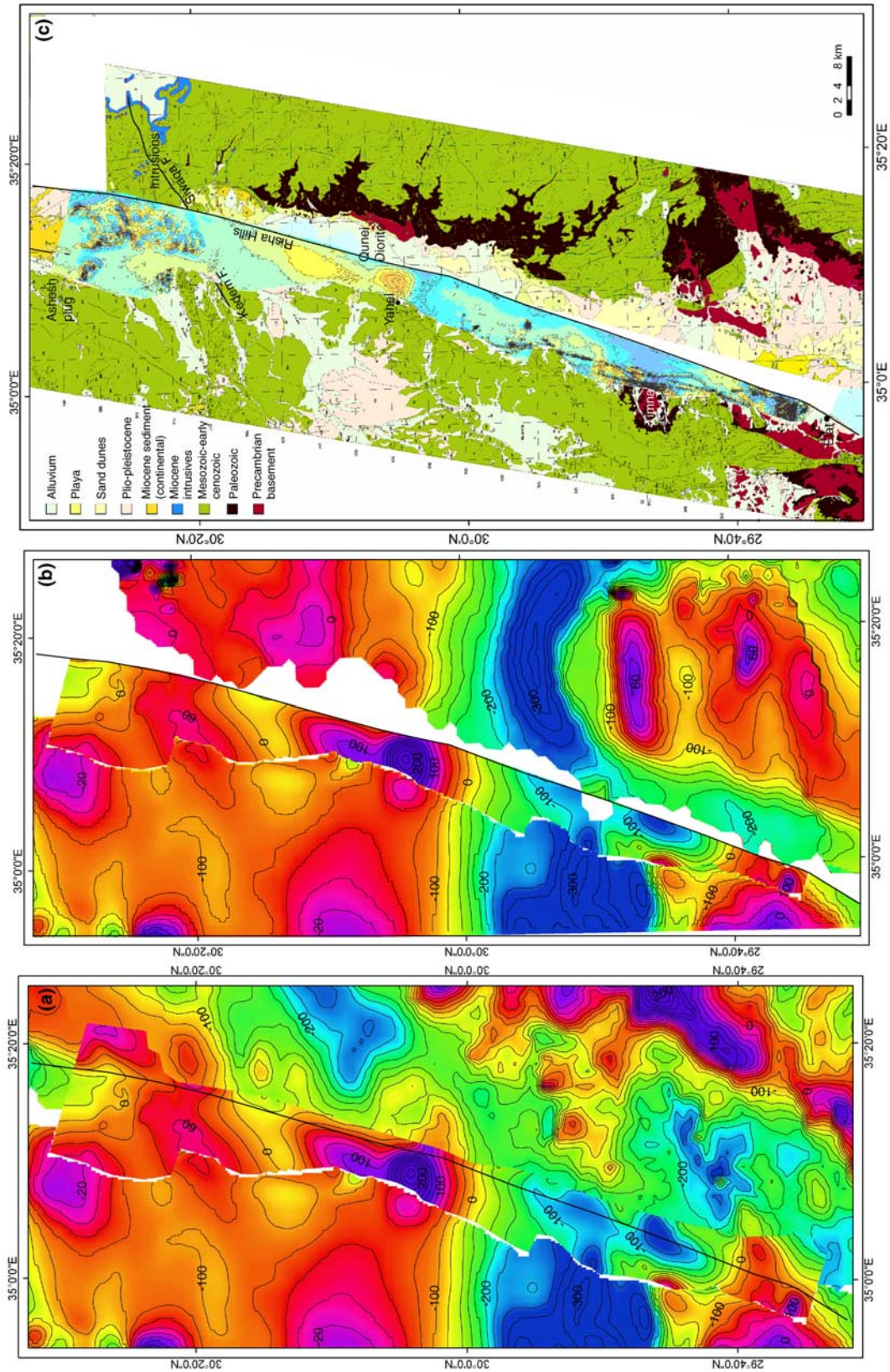
Figure 3

under the transform valley, associated with a leaky transform [*Garfunkel*, 1981; *Schubert and Garfunkel*, 1984]. Transform-normal extension was suggested as an alternative explanation to pull-apart models within the Dead Sea transform [*Ben-Avraham and Zoback*, 1992]. The magnetic data show no evidence for igneous activity that post-dates the beginning of displacement in this segment of the Dead Sea Transform, despite the presence of basins underlying the transform valley in this area [*ten Brink et al.*, 1999].

[17] A few locations within the transform valley are associated with positive magnetic anomalies, which are likely related to shallow magnetic sources (Figure 2a). In these areas, the Arava Fault trace separates anomalies of different character and likely different origins. In the northern part of the survey region (between latitudes 30°23′N and 30°27.5′N), the Arava Fault separates a region of high-frequency magnetic anomalies in the west from a NNE trending linear anomaly in the east (Figures 2a and 2c). The anomalies in the east probably represent buried Precambrian rocks such as the Aheimir metavolcanic, which are exposed nearby. The anomalies in the west probably represent pretransform Neogene-age buried volcanic flows or magmatic intrusions [*Frieslander*, 2000], extrapolating from a nearby (Figure 1a) small magmatic outcrop (the 20.7 Ma Ashosh plug [*Steinitz et al.*, 1978]). The Ashosh Plug is located at the northern edge of the dike system that was formed during the early opening of the Red Sea prior to the initiation of motion on the Dead Sea Transform [*Baldridge et al.*, 1991]. Basic intrusions of a similar age (19 Ma) are exposed along the eastern highlands 100–110 km to the north [*Barberi et al.*, 1980], and they form a NW-SE (Red Sea-parallel) trend with the mapped high frequency anomalies and with the Ashosh Plug, when they are shifted south by the total slip along the Dead Sea Transform (Figure 3c).

[18] The western boundary of these magnetic anomalies extends south of the surface expression of the Zofar Fault (Figures 1 and 2c). The Zofar fault is a secondary fault of the Dead Sea Transform, which vertically offsets basin fill in outcrops north of our survey area [*Bartov et al.*, 1998]. Seismic reflection data within our survey area show the fault as having vertical offsets with the east side down [*Frieslander*, 2000].

[19] The southern boundary of the zone of high frequency magnetic anomalies appears to be the continuation of the Kedem Fault, a NE-oriented

fault west of our survey area, which has no surface expression [*Frieslander*, 2000]. The boundary is sharp and linear, presumably expressing a fault line. When the eastern side of the transform is restored to its pretransform position 107 km southward, this fault appears to be continuous with the Siwaqa fault (Figure 3c), a large fault in central Jordan that predates the transform [*Bender*, 1974, pp. 113–114].

[20] A high amplitude positive anomaly, centered at Lat. 30°05.5′ (near Yahel) terminates against the Arava Fault (Figures 2 and 3c). A lesser positive anomaly extends about 10 km to the NNW parallel to the trend of the Arava Fault. There are no magnetic outcrops nearby, but seismic reflection profiles along the western edge of the transform valley [*Frieslander*, 2000], gravity anomalies (Figure 2b), and outcrops of pretransform rocks within the valley (Figure 1a) indicate that crystalline basement is probably shallower here than in the surrounding areas. The anomaly is either quite wide or quite deep, because it is amplified in the magnetic field, which is upward continued to 3000 ft. (Figure 3a). However, part of the contribution to the positive anomaly arises from a more regional contribution (Figure 3a), which is discussed below. A source candidate for this anomaly is the Precambrian Qunei diorites [*Sneh et al.*, 1998] with susceptibility $\leq 20 \times 10^{-3}$ SI (M. Rybakov, unpublished data, 2003) or, generally a more shallow crystalline basement, both of which are exposed on the east side of the transform ~111 km to the north, an equivalent distance to left-lateral offset of the Dead Sea Transform since its inception (Figure 3c).

[21] At Lat. 29°39–29°42′, the Arava Fault passes at the center of the valley, separating higher frequency anomalies west of the fault from lower frequency anomalies east of it (Figures 1 and 2). The anomalies west of the fault are probably due to continuation of Precambrian quartz-diorite rocks that crop out nearby (Roded Formation [*Sneh et al.*, 1998]). Magnetic anomalies east of the fault correspond, most probably, to Precambrian Duhayla hornblendite that are exposed nearby [*Sneh et al.*, 1998].

3.4. Magnetic Anomalies and Sedimentary Basins

[22] Negative magnetic anomalies observed on the total magnetic intensity map (TMI) are interpreted to define local sedimentary basins (Figures 2a and 2b). On the basis of gravity data [*ten Brink et al.*, 1999], these basins appear to be relatively
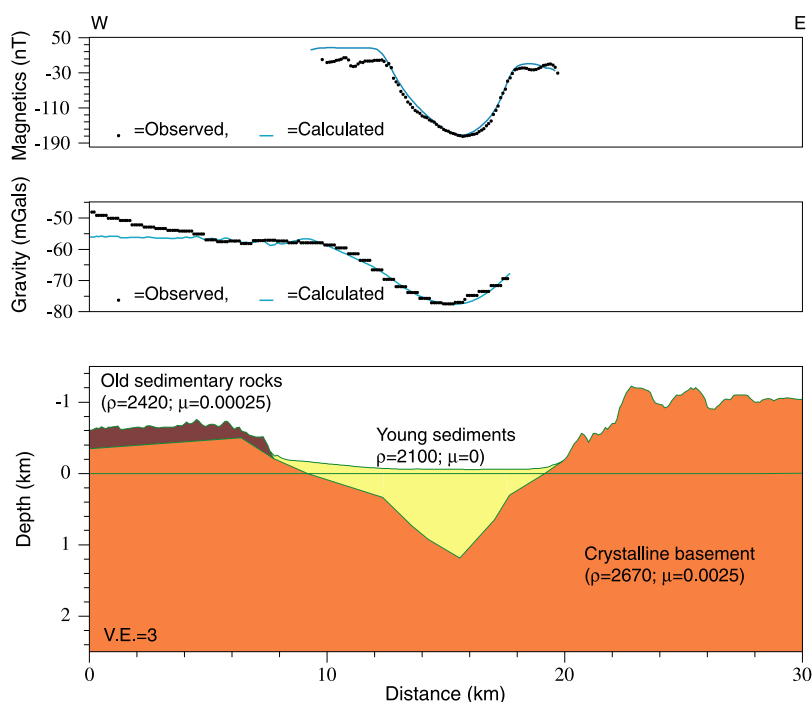
Figure 4. Shape and depth of Timna Basin calculated from a joint 2-D magnetic and gravity model across Arava Valley. Location of profile is shown in Figure 2a. ρ, density; μ, susceptibility in SI units.

shallow (0.5–1.5 km), occupy only part of the width of the transform valley, and are filled with relatively non-magnetic sediment surrounded by more magnetic crystalline basement rocks. Comparison between the TMI map and the gravity map shows good correspondence between many of the negative gravity and magnetic anomalies (Figure 2b). The correspondence is particularly good in the Timna basin (lat. 29°47′N), the largest of the sedimentary basins in the southern Arava valley, where a coincident gravity and magnetic cross-section can be modeled by a sedimentary basin reaching a maximum depth of 1.2 km (Figure 4). Gravity and magnetic anomalies also correspond in the Aqaba basin at the southern end of the survey area, in the narrow Gharandal Basin (30°10′N), in a remnant pretransform basin farther north (30°18′) and at the southern end of the Dead Sea basin (30°30′N) (Figures 2b). Thus the details of the magnetic map often appear to qualitatively reflect the depth to crystalline basement.

4. Discussion: Why Is the Fault Zone Visible in the Aeromagnetic Data?

[23] The Arava Fault is clearly observed in the FVD of the magnetic intensity map (Figures 2c and 2d). The map is gridded at 75 m intervals; hence the expression of the fault zone covers at least 2–3 grid points or 150–225 m wide zone. A more quantitative estimate of the fault zone width is discussed below.

[24] Some sections of the Arava fault, which separate zones of positive magnetic anomalies (e.g., between lat. 30°23′ and 30°27.5′, at Lat. 30°04′, and between Lat. 29°39 and 29°42′; see Figure 2a for location), are delineated by a 1–2 km-wide negative anomaly with amplitude of 10–20 nT (Figure 5). Assuming that the anomalies are due to induced magnetization, we inverted the anomaly for the magnetic susceptibility along two flight lines, 1056 and 1344, which cross the fault in these areas. We used a linear inversion method [*Webring*, 1985] as implemented in GM-SYS™ and inverted for a 3-km thick source layer, below the surface topography. We chose a 3-km-thick layer, being the maximum depth of perturbations to density, *P* wave velocity, and electrical conductivity of the shallow fault zone in the San Andreas Fault [*Hole et al.*, 2001]. The inversion indicates lower magnetic susceptibility in a 1.5–2 km wide zone (Figure 5). This could be the result of fault processes and/or groundwater that have altered magnetic minerals to less magnetic phases, such as magnetite to hematite.

[25] A high-resolution seismic reflection survey across the fault near line 1056 (at latitudes 29°38.5′–
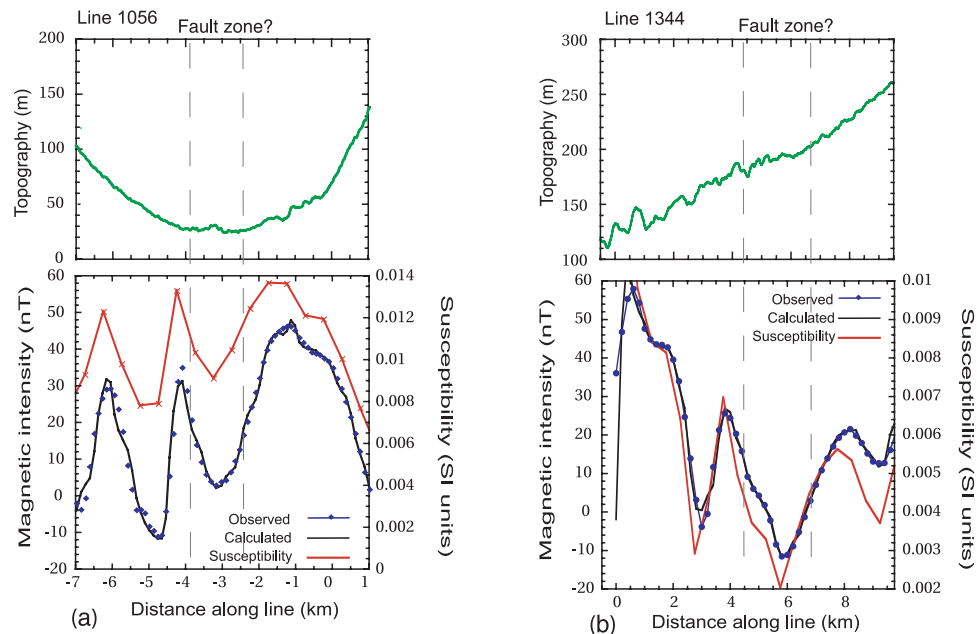
Figure 5. (a) (bottom) Observed and calculated magnetic anomaly along flight line 1056, and the calculated magnetic susceptibility along the line assuming a 3-km-thick layer of variable susceptibility. (top) Topography along line measured by the helicopter. See Figure 2a for line location. Magnetic anomaly and susceptibility were calculated using the program GMSYS™. (b) Same as in Figure 5a for data and model along flight line 1344.

29°40.5′), reveals up to three parallel fault traces within a 1200 m wide zone [*Shtivelman et al.*, 1998]. The faults appear as "flower structures" extending from a few meters below the surface to a maximum depth of ~150 m. Trenches in that area reveal numerous Holocene normal offsets within 5 m of the surface in a 1200 m wide area [*Amit et al.*, 2002]. Hence the 1–2 km wide fault zone, seen in the seismic and magnetic data, is perhaps a zone through which numerous fault traces have been active either simultaneously or at different times. Whether this wide fault zone extends deeper than the shallow subsurface is unknown.

[26] The fault trace can also be followed in areas not surrounded by magnetic bodies, such as in the Timna Basin (lat. 29°47′N), and the Risha Hills (lat. 30°15′N) (see Figures 1 and 2 for location). In these areas, the fault trace is associated with a small positive anomaly, superposed on a larger regional trend. When the trend is removed, a 1–4 nT positive anomaly is revealed (Figure 6). This small signal can be inverted assuming a 100-m thick surficial alluvial layer. The inversion indicates a small positive variation in susceptibility across a 0.7–1 km wide zone (Figure 6).

[27] Enhancement of magnetic susceptibility of soils is probably due to the formation of magnetite and maghemite from the precipitation of iron and

soil solutions [*Singer et al.*, 1996]. Higher susceptibility within the fault zone could arise from iron oxide cementation due to groundwater circulation in the fault zone. Lines of vegetation and shallow groundwater are observed along the fault north of our study area [*Garfunkel et al.*, 1981; *Kesten*, 2004]. Although the area is arid, groundwater is recharged from surface flow from the eastern highlands and fossil groundwater from the western highland, and flows southward along the valley axis into the Gulf of Aqaba [*Bein et al.*, 2001]. Local earthquakes appear capable of temporarily altering the hydrologic regime of this arid area, increasing groundwater heads and spring discharge [*Yechieli and Bein*, 2002]. Geochemical studies in the Arava valley north of our survey area indicate fluid infiltration into the shallow fault zone [*Janssen et al.*, 2004].

[28] A coincidence of faults with magnetic lineaments has been previously observed elsewhere and was interpreted in different ways. *Peirce et al.* [1998] claimed that roughly 25% of the seismically visible faults in their study area can be detected magnetically, but numerous fractures, not detected seismically, can also be seen in HRAM surveys. They attributed their observations to exotic minerals being deposited in faults and fractures by redox processes induced by vertical flow of water [*Pierce*
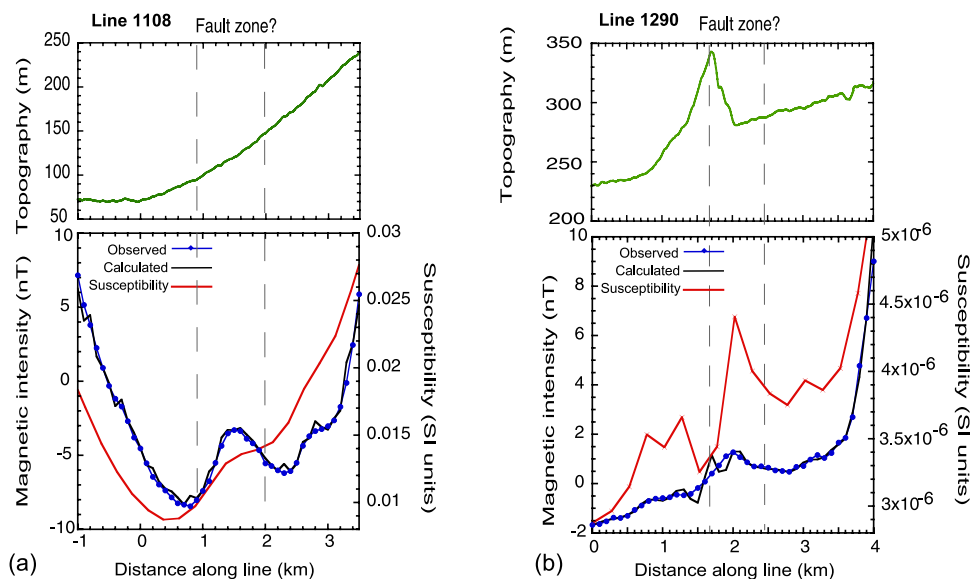
Figure 6. (a) (bottom) Observed and calculated magnetic anomaly along flight lines 1108 and the calculated magnetic susceptibility along these lines assuming a 100-m-thick layer of variable susceptibility. A linear trend was removed from the observed magnetic anomaly prior to modeling. (top) Topography along these lines measured by GPS and the helicopter altimeter. See Figure 2a for line locations. Magnetic anomaly and susceptibility were calculated using the program GMSYS™. (b) Same as in Figure 6a for data and model along flight line 1290.

et al., 1998]. *Blakely et al.* [2004] and *Sherrod et al.* [2005] have interpreted buried reverse faults in the Puget Sound area, Washington, from HRAM data, ground magnetic surveys, susceptibility measurements and trenching. Their favored explanation for the source of the anomalies is faulted offsets in the underlying Pleistocene strata, although they could not discount other explanations, such as secondary magnetic minerals along buried fractures or faults, possibly related to elevated groundwater levels, or lateral variations in magnetic properties due to contrasting lithologies within the glacial sediments. *Grauch et al.* [2001] mapped normal faults within the Albuquerque basin using HRAM. They concluded that the fault signature, which is often expressed as a step in the magnetic field, is due to juxtaposition of two magnetic bodies at different depths, and not due to hydrologically concentrated magnetic minerals. In support of their conclusion, they presented ground magnetic intensity and susceptibility profiles across a 140 m wide cemented fault zone that showed no effect of the cemented zone. Similar data in our survey area do not exist, and its usefulness is doubtful, because the ground is covered by thick unconsolidated fluvial and eolian sediments.

[29] The fault-associated anomaly in our study area appears to be limited to the major active fault in the area. This suggests that a dynamic process, such as groundwater recharge along the shallow fault zone, may play a role in altering the magnetic intensity field. If the source of the anomaly is shallow, as indicated by its visibility on the FVD data, then the source of the magnetic anomaly must be several hundreds of meters wide.

[30] This implies that the shallow fault width is at least several hundred meters wide, in agreement with seismic reflection data [*Shtivelman et al.*, 1998; *Haberland et al.*, 2007], trenching [*Amit et al.*, 2002], and geochemical analysis [*Janssen et al.*, 2004]. The lack of surface expression for the fault in this segment of the Dead Sea Transform, which was active as late as 1458 AD [*Klinger et al.*, 2000a], may reflect velocity strengthening during an earthquake [e.g., *Marone*, 1998], resulting in little or no surface rupture. It is less likely that coverage by recent sediments has obscured the fault trace, because of the low rate of sediment supply in this extremely arid area.

5. Conclusions

[31] A high-resolution aeromagnetic survey over a 120-km-long segment of the Dead Sea transform valley demonstrates the utility of such surveys in the study of large active faults. The survey reveals

an almost continuous fault trace along the transform valley in the survey area. The fault can be traced even in areas that are devoid of significant magnetic sources, by using high-frequency low amplitude anomalies whose source is likely to lie within the sedimentary cover. Modeling of these anomalies indicates a fault zone several hundreds meter wide. Processes related to active motion, such as groundwater recharge, may introduce magnetic minerals in non-magnetic areas along the fault, and reduce the strength of the anomaly, where the fault zones cuts through the crystalline basement. The wide fault zone at the surface may be indicative of velocity strengthening and the near-absence of surface rupture during earthquakes in this fault segment.

[32] The longer wavelength magnetic anomalies within the transform valley appear to be continuous with the magnetic field west of the valley, and discontinuous with the field east of the valley, indicating that the plate boundary was always located at the Arava Fault or perhaps east of it, but never to the west. Magnetic anomalies due to igneous sources related to the plate boundary motion were not identified within the transform valley. In areas devoid of magnetic sources, negative magnetic anomalies appear to correlate with depth to buried crystalline basement within the transform valley.

Acknowledgments

References

Aldersons, F., Z. Ben-Avraham, A. Hofstetter, E. Kissling, and T. Al-Yazjeen (2003), Lower-crustal strength under the Dead Sea basin from local earthquake data and rheological modeling, *Earth Planet. Sci. Lett.*, *214*, 129–142.

Al-Zoubi, A., and Z. Ben-Avraham (2002), Structure of the Earth's crust in Jordan from potential field data, *Tectonophysics*, *346*, 45–59.

Amit, R., E. Zilberman, Y. Enzel, and N. Porat (2002), Paleoseismic evidence for time dependency of seismic response on a fault system in the southern Arava Valley, Dead Sea Rift, Israel, *Geol. Soc. Am. Bull.*, *114*, 192–206.

Baldridge, W. S., Y. Eyal, Y. Bartov, G. Steinitz, and M. Eyal (1991), Miocene magmatism of Sinai related to the opening of the Red Sea, *Tectonophysics*, *197*, 181–201.

Barberi, F., G. Capaldi, P. Gasperini, G. Marinelli, R. Santacroce, R. Scandone, M. Treuil, J. Varet, and A. Carrelli (1980), Recent basaltic volcanism of Jordan and its implications on the geodynamic history of the Dead Sea shear zone, in *Atti dei Convegni Lincei*, vol. 47, pp. 667–683, Accad. Naz. dei Lincei, Rome.

Bartov, Y., Y. Avni, R. Calvo, and U. Frieslander (1998), The Zofar fault—A major intra-rift feature in the Arava rift valley, *Geol. Surv. Isr. Current Res.*, *11*, 27–32.

Bein, A., Y. Yechieli, and J. Bensabat (2001), Quantifying the groundwater resources of the southern Arava rift valley: A confined desert system recharged laterally by external sources, *Isr. J. Earth Sci.*, *50*, 217–236.

Ben-Avraham, Z., and M. D. Zoback (1992), Transform-normal extension and asymmetric basins: An alternative to pull-apart models, *Geology*, *20*, 423–426.

Bender, F. (1974), *Geology of Jordan*, 196 pp., Borntraeger, Berlin.

Blakely, R. J. (1995), *Potential Theory in Gravity and Magnetic Applications*, Cambridge Univ. Press, New York.

Blakely, R. J., B. L. Sherrod, R. E. Well, C. S. Weaver, D. H. McCormack, K. G. Troost, and R. A. Haugerud (2004), The Cottage Lake aeromagnetic lineament: A possible onshore extension of the southern Whidbey Island fault, Washington, *U.S. Geol. Surv. Open File Rep.*, *2004–1204*, 60 pp.

Chester, F. M., J. P. Evans, and R. L. Biegel (1993), Internal structure and weakening mechanisms of the San Andreas Fault, *J. Geophys. Res.*, *98*, 771–786.

Domzalski, W. (1967), Aeromagnetic survey of Israel interpretation, report, 62 pp., Inst. Petrol. Res. Geophys., Holon, Israel.

Fialko, Y., D. Sandwell, M. Simons, and P. Rosen (2005), Three-dimensional deformation caused by the BAM, Iran, earthquake and the origin of shallow slip deficit, *Nature*, *435*, 295–299.

Freund, R., Z. Garfunkel, I. Zak, M. Goldberg, T. Weissbrod, and B. Derin (1970), The shear along the Dead Sea rift: A discussion on the structure and evolution of the Red Sea and the nature of the Red Sea, Gulf of Aden and Ethiopia rift junction, *Philos. Trans. R. Soc. London, Ser. A*, *267*, 107–130.

Frieslander, U. (2000), The structure of the Dead Sea transform emphasizing the Arava using new geophysical data, Ph.D. thesis, 101 pp., The Hebrew Univ., Jerusalem.

Garfunkel, Z. (1981), Internal structure of the Dead Sea leaky transform (rift) in relation to plate kinematics, *Tectonophysics*, *80*, 81–108.

Garfunkel, Z., I. Zak, and R. Freund (1981), Active faulting in the Dead Sea Rift, *Tectonophysics*, *80*, 1–26.

Ginat, H., Y. Enzel, and Y. Avni (1998), Translocated Plio-Pleistocene drainage systems along the Arava Fault of the Dead Sea Transform, *Tectonophysics*, *284*, 151–160.

Grauch, V. J. S., M. R. Hudson, and S. A. Minor (2001), Aeromagnetic expression of faults that offset basin fill, Albuquerque basin, New Mexico, *Geophysics*, *66*, 707–720.

Haberland, C., A. Agnon, R. El-Kelani, N. Maercklin, I. Qabbani, G. Rümpker, T. Ryberg, F. Scherbaum, and M. Weber (2003), Modeling of seismic guided waves at the Dead Sea Transform, *J. Geophys. Res.*, *108*(B7), 2342, doi:10.1029/2002JB002309.

Haberland, C., N. Maercklin, D. Kesten, T. Ryberg, Ch. Jannsen, A. Agnon, M. Weber, A. Schulze, I. Qabbani, and R. El-Kelani (2007), Shallow architecture of the Wadi Araba fault (Dead Sea Transform) from high-resolution seismic investigations, *Tectonophysics*, *432*, 37–50.

Hatcher, R. D., Jr., I. Zietz, R. D. Regan, and M. Abu-Ajamieh (1981), Sinistral strike-slip motion on the Dead Sea Rift; confirmation from new magnetic data, *Geology*, *9*, 458–462.

Hole, J. A., R. D. Catchings, K. C. St Clair, M. J. Rymer, D. A. Okaya, and B. J. Carney (2001), Steep-dip seismic imaging of the shallow San Andreas Fault near Parkfield, *Science*, *294*, 1513–1515.

Janssen, C., R. L. Romer, A. Hoffmann-Rothe, D. Kesten, and H. Al-Zubi (2004), The Dead Sea Transform: Evidence for a strong fault?, *J. Geol.*, *112*, 561–575.

Kesten, D. (2004), Structural observations at the southern Dead Sea transform from seismic reflection data and ASTER satellite images, 96 pp., Potsdam Univ., Ph.D. thesis, Potsdam, Germany.

Klinger, Y., J. P. Avouac, N. Abou Karaki, L. Dorbath, D. Bourles, and J. L. Reyss (2000a), Slip rate on the Dead Sea transform fault in northern Araba Valley (Jordan), *Geophys. J. Int.*, *142*, 755–768.

Klinger, Y., J. P. Avouac, L. Dorbath, N. Abou Karaki, and N. Tisnerat (2000b), Seismic behaviour of the Dead Sea Fault along Araba Valley, Jordan, *Geophys. J. Int.*, *142*, 769–782.

Mahmoud, S., R. Reilinger, S. McClusky, P. Vernant, and A. Tealeb (2005), GPS evidence for northward motion of the Sinai block: Implications for E. Mediterranean tectonics, *Earth Planet. Sci. Lett.*, *238*, 217–224.

Marone, C. (1998), Laboratory-derived friction laws and their application to seismic faulting, *Annu. Rev. Earth Planet. Sci.*, *26*, 643–696.

Peirce, J. W., S. A. Goussev, R. A. Charters, H. J. Abercrombie, and G. R. DePaoli (1998), Intrasedimentary magnetization by vertical fluid flow and exotic geochemistry, *Leading Edge*, *18*, 89–92.

Quennell, A. M. (1958), The structural and geomorphic evolution of the Dead Sea rift, *Q. J. Geol. Soc London, 114, Part 1*, 1–24.

Ritter, O., T. Ryberg, U. Weckmann, A. Hoffmann-Rothe, A. Abueladas, and Z. Garfunkel, and DESERT Research Group (2003), Geophysical images of the Dead Sea Transform in Jordan reveal an impermeable barrier for fluid flow, *Geophys. Res. Lett.*, *30*(14), 1741, doi:10.1029/2003GL017541.

Rybakov, M., V. Goldshmidt, and Y. Rotstein (1997), New regional gravity and magnetic maps of the Levant, *Geophys. Res. Lett.*, *24*, 33–36.

Savage, J. C., and M. Lisowski (1993), Inferred depth of creep on the Hayward Fault, central California, *J. Geophys. Res.*, *98*, 787–793.

Schubert, G., and Z. Garfunkel (1984), Mantle upwelling in the Dead Sea and Salton Trough-Gulf of California leaky transforms, *Ann. Geophys.*, *2*, 633–648.

Segev, A., V. Goldshmidt, and M. Rybakov (1999), Late Precambrian-Cambrian tectonic setting the crystalline basement in the northern Arabian-Nubian Shield as derived from gravity and magnetic data; basin and range characteristics, *Isr. J. Earth Sci.*, *48*, 159–178.

Sherrod, B. L., R. J. Blakely, C. S. Weaver, H. Kelsey, E. Barnett, and R. E. Well (2005), Holocene fault scarps and shallow magnetic anomalies along the southern Whidbey Island fault zone near Woodinville, Washington, *U.S. Geol. Surv. Open File Rep.*, *2005–1136*, 36 pp.

Shtivelman, V., U. Frieslander, E. Ziberman, and R. Amit (1998), Mapping shallow faults at the Evrona playa site using high-resolution reflection method, *Geophysics*, *63*, 1257–1264.

Singer, M. J., K. L. Verosub, P. Fine, and J. TenPas (1996), A conceptual model for the enhancement of magnetic susceptibility in soils, *Quat. Int. J.*, *34–36*, 2443–2458.

Sneh, A., Y. Bartov, T. Weissbrod, and M. Rosensaft (1998), Geological map of Israel, scale 1:200000, Geol. Surv. of Isr., Jerusalem.

Steinitz, G., Y. Bartov, and J. C. Hunziker (1978), K-Ar age determinations of some Miocene-Pliocene basalts in Israel: Their significance to the tectonics of the rift valley, *Geol. Mag.*, *115*, 329–340.

ten Brink, U. S., M. Rybakov, A. Al-Zoubi, M. Hassouneh, A. Batayneh, U. Frieslander, V. Goldschmidt, M. Daoud, Y. Rotstein, and J. K. Hall (1999), Anatomy of the Dead Sea Transform: Does it reflect continuous changes in plate motion?, *Geology*, *27*, 887–890.

Unsworth, M., P. Bedrosian, M. Eisel, G. Egbert, and W. Siripunvaraporn (2000), Along strike variations in the electrical structure of the San Andreas Fault at Parkfield, California, *Geophys. Res. Lett.*, *27*, 3021–3024.

Wdowinski, S., Y. Bock, G. Baer, L. Prawirodirdjo, N. Bechor, S. Naaman, R. Knafo, Y. Forrai, and Y. Melzer (2004), GPS measurements of current crustal movements along the Dead Sea Fault, *J. Geophys. Res.*, *109*, B05403, doi:10.1029/2003JB002640.

Webring, M. (1985), SAKI: A Fortran program for generalized linear inversion of gravity and magnetic profiles, *U.S. Geol. Surv. Open File Rep.*, *85–122*.

Yechieli, Y., and A. Bein (2002), Response of groundwater systems in the Dead Sea Rift Valley to the Nuweiba earthquake: Changes in head, water chemistry, and near-surface effects, *J. Geophys. Res.*, *107*(B12), 2332, doi:10.1029/2001JB001100.